Supporting Information

Expanding the Range of Graphene Energy Transfer with Multilayer Graphene

Karolina Gronkiewicz[1], Lars Richter[2], Fabian Knechtel[2], Patryk Pyrcz[1], Paul Leidinger[3,4], Sebastian Günther[3], Evelyn Ploetz[2], Philip Tinnefeld[2]*, Izabela Kamińska[1,2]*

[1] Institute of Physical Chemistry of the Polish Academy of Sciences, Kasprzaka 44/52, 01-224 Warsaw, Poland

[2] Department of Chemistry and Center for NanoScience, Ludwig Maximilian University of Munich, Butenandtstraße 5-13, 81377 Munich, Germany

[3] Department of Chemistry, Technical University of Munich (TUM), Catalysis Research Center, Lichtenbergstraße 4, 85748 Garching, Germany

[4] Current address: Paul Scherrer Institut, 5232 Villigen PSI, Switzerland

Corresponding Authors

* E-mail: izabela.kaminska@lmu.de, philip.tinnefeld@lmu.de

Table of Contents

1. Materials and Methods

1.1. Buffers and recipes

If no other company is mentioned, chemicals were purchased from Sigma Aldrich.

Table S1. The list of buffers with recipes.

Name	Recipe
FOB20	20 mM $MgCl_2 \cdot 6H_2O$ 20 mM Tris base 20 mM acetic acid 1 mM EDTA-$Na_2 \cdot 2\ H_2O$
FOB12.5	12.5 mM $MgCl_2 \cdot 6H_2O$ 20 mM Tris base 20 mM acetic acid 1 mM EDTA-$Na_2 \cdot 2\ H_2O$
PCA/Trolox12	2 mM Trolox (6-hydroxy-2,5,7,8-tetramethylchroman-2-carboxylic acid) 25 mM PCA (protocatechuic acid) 12 mM $MgCl_2 \cdot 6H_2O$ 40 mM Tris base 20 mM acetic acid 1 mM EDTA-$Na_2 \cdot 2H_2O$
50× PCD	2.8 mM PCD (protocatechuate 3,4-dioxygenase from pseudomonas sp.) 50% glycerol 50 mM KCl 100 mM Tris HCl 1 mM EDTA-$Na_2 \cdot 2H_2O$

1.2. Preparation of monolayer and multilayer graphene-on-glass coverslips

CVD-grown monolayer and multilayer graphene deposited on copper foil covered with poly (methyl methacrylate) (PMMA) was purchased from Graphenea® and ACS Material®. The wet-transfer method was employed to transfer the graphene onto glass coverslips.[1] Each coverslip was cleaned by sonicating at room temperature, in 1 % aqueous solution of Hellmanex (Hellma®), and then twice in MilliQ water, every step for 15 minutes. Small pieces, of approximately 0.25 cm^2 in size, were cautiously cut from the PMMA/Gr/Cu foil. The copper underwent wet etching by letting a piece float with the copper film exposed to 0.2 M ammonium persulfate for ~4 hours. A coverslip was carefully immersed vertically and moved slowly towards the PMMA/Gr, then gently scooped out of the solution. It was subsequently transferred to MilliQ water to rinse off any remaining residues of ammonium persulfate. Another layer of liquid PMMA (M_w = 120,000 g/mol) dissolved in chlorobenzene (50 mg/mL) was drop-casted onto the initial PMMA/Gr layer. This allowed the re-dissolution of the dried PMMA, thereby relaxing the underlying graphene monolayer and enhancing the contact with the substrate.[1] After 30 minutes, the PMMA/Gr on glass underwent a sequential immersion process: twice in

fresh acetone for 5-10 minutes, and then in toluene for 5-10 minutes. After the second cleaning step in acetone and in toluene, the samples were gently dried with a nitrogen stream. Finally, the sample was placed on active coal, heated on a heating plate at 230 °C for 8 hours, and then allowed to gradually cool down. To prepare bilayer (trilayer) graphene, both transfer and cleaning protocols described above were repeated twice (trice) subsequently. After removing the PMMA from the initially transferred graphene layer, we placed on top of it another monolayer graphene (Cu etched and PMMA/Gr washed in MilliQ water beforehand, as described above), ensuring complete coverage of the graphene sheets. Notably, we intentionally applied the second (third) layer slightly larger than the bottom layer to minimize the formation of defects and to ensure a full overlap of both (all three) graphene layers.

1.3. Preparation of DNA origami structures

DNA origami nanostructures were designed using caDNAno, employing the p8064 scaffold derived from M13mp18 bacteriophages. DNA origami structures were folded using a 10-fold surplus of unmodified and internally labeled oligonucleotides, along with a 100-fold excess of biotinylated or pyrene-modified oligonucleotides in comparison to the scaffold in FOB20 buffer. The folding program specifics can be found in ref.[2]. After the folding, 1× Blue Juice gel loading buffer was added to the DNA origami solution, followed by purification through agarose-gel electrophoresis with 1.5 % agarose gel in 50 mL of FOB12.5 buffer (peqGREEN (VWR) 2 µL/100 µL of buffer, 70 V for 1.5 h). The specific band for the nanostructure was extracted from the gel. Prior to application onto glass or graphene, the concentration of the purified DNA origami solution was adjusted with FOB12.5 buffer to 50 pM. The positions and distances of dyes in DNA origami structures were estimated based on a presumed distance of 0.34 nm between nucleotides along the DNA double helix and 2.7 nm between the centers of adjacent helices within a square lattice, as outlined in references.[3,4] Any discrepancies from the estimated values may arise from the slight bending or tilting of DNA origami nanostructures.[5] It is also important to take into account that variations between the designed and measured distances may be influenced by the specific structure, interactions between the dye and DNA, as well as the salt concentration.

2. Imaging and Analysis

2.1. Fluorescence confocal microscope

Single-molecule fluorescence measurements were performed on a home-built confocal setup based on an Olympus IX71 microscope. The green laser (LDH-P-FA-530B, Picoquant) is

controlled by a PDL 828 “Sepia II” (Picoquant). The green fiber (polarization maintaining fiber with FC/APC output connector) coupled laser light is decoupled via a F220APC-532 collimator (Thorlabs) and cleaned up with a 532/2 (Z532/10 X, Chroma) filter before passing a dichroic mirror (640 LPXR, Chroma) for optional combination with the already cleaned up (Z640/10 X, Chroma) red laser (LDH-D-C-640, Picoquant). A linear polarizer (WP12L-Vis, Thorlabs) and a quarter-wave plate (AQWP05M-600, Thorlabs) are combined to obtain circularly polarized light. After passing a second dichroic mirror (zt532/640rpc, Chroma) the beam is focused via an oil immersion objective (UPLSAPO 100 XO, NA 1.40, Olympus) onto the sample. The sample is scanned with a piezo-stage (P-527.3CD, Physik Instrumente) which is controlled by an E-727 controller (Physik Instrumente). The emitted light is focused on a 50 µm pinhole (Thorlabs) and collimated with a lens (AC050-150-A-ML, Thorlabs). The TCSPC module data was analyzed using a custom-written Python software, smPyFLIM.[6] This software comprises two modules: one for analyzing time traces and another for opening and processing FLIM images. The necessary scripts to initiate the graphical user interfaces (GUI) are available at https://github.com/alanszalai/smPyFLIM.

2.2. Raman spectrometers

The investigation of the graphene substrates, mapping, and spectra measurements (Figure S1 – S3), was carried out on a confocal scanning Raman microscope. The setup operates with a continuous-wave diode laser (Cobolt SambaTM100 04-01 Series, Cobalt) with a maximum output of 100 mW at 532 nm. A dichroic (zet532/NIR, AHF Analysentechnik) separates the excitation from the detection beam inside of the microscope body (TE 300, Nikon). An air objective (Plan APO 60× 0.95 NA, Nikon) focuses the laser on the sample. With an air objective, measurements of > 10 h are possible without losing the focus. The Rayleigh scattering is blocked by a 532 notch and a 537 longpass filter. The signal is detected on a spectrometer (Kymera 328i, Oxford Instruments). The Raman spectra were measured with a 300 lines per mm grating (centered at 598 nm) for 2 seconds with an electronic gain of 150. The layer-by-layer samples were scanned by 160 × 160 lines with a size of 65 × 65 µm and the CVD-grown bilayer sample by 210 × 210 lines with a size of 80 × 80 µm.

Measurements of Raman spectra (Figure S4a, S4c) were conducted on a Raman spectrometer (InVia Renishaw) with an integrated microscope (Leica), which was equipped with a thermoelectrically cooled 1024 × 256 pixels CCD detector and a bright single monochromator. Raman spectra were gathered for each measurement position during raster scanning of a sample

in the horizontal (XY) plane. The Raman spectra were acquired under 632.8 nm excitation using a 50× Leica objective (NA = 0.75) and were dispersed by 1200 l/mm holographic gratings in the visible spectral range. The acquisition time per pixel was set to 20 s with an excitation power of 1 mW. Renishaw Wire 5.6 software was employed to correct the data against cosmic rays, derive the intensity distribution for graphene peaks, and calculate the average of the collected data.

2.3. Scanning electron microscope

The Nova NanoSEM 450 scanning electron microscope (SEM) was used to investigate both the number of graphene layers and their quality (Figure S4b and S5). To prepare the substrate for SEM measurement, small pieces of a silicon wafer (approximately 1 cm^2) were sonicated in a 0.5 % Hellmanex™ III solution for 15 minutes at 50 °C, followed by sonication in deionized water (15 minutes, 50 °C) to remove any residues of the alkali solution from the substrates. Graphene was deposited on top using the method mentioned previously.[1] After PMMA removal, samples were mounted on SEM specimen stubs with copper. Graphene samples were characterized at a voltage of 10 kV in immersion mode.

3. Experiments

3.1. Calculations

The energy transfer efficiency η is defined as:

$$\eta = \frac{k_{GET}}{k_{GET} + \sum k_i}$$

with $\sum k_i$ being the sum of all other depopulating rates unaffected by the acceptor (graphene). The graphene energy transfer rate is defined as:

$$k_{GET} = \frac{1}{\tau_{ref}} \left(\frac{d}{d_0}\right)^4$$

With τ_{ref} as donor lifetime without acceptor, d is the distance between the emitter and graphene, d_0 distance of the 50% energy transfer efficiency which equals to 17.7 ± 0.5 nm for a green dye molecule and 18.5 ± 0.7 nm for a red dye molecule, respectively.[7]

If we combine both equations:

$$\eta = \frac{\frac{1}{\tau_{ref}} \left(\frac{d}{d_0}\right)^4}{\frac{1}{\tau_{ref}} \left(\frac{d}{d_0}\right)^4 + \sum k_i} = \frac{1}{1 + \sum k_i \cdot \tau_{ref} \cdot \left(\frac{d}{d_0}\right)^4} = \frac{1}{1 + \left(\frac{d}{d_0}\right)^4}$$

Because of $\tau_{ref} = \frac{1}{\sum k_i}$.

In our model, we assume that every additional graphene layer exhibits the same quenching behavior, and considering weak interaction between the layers, we also assume that multilayer graphene is simply a stack of decoupled monolayer graphene sheets.[8] Other factors, such as the interactions between the graphene layers, are neglected. If we assume, that k_{GET} rates add up with the number of graphene layers and we neglect the interlayer spacing:

$$\eta = \frac{n \cdot k_{GET}}{n \cdot k_{GET} + \sum k_i} = \frac{n \cdot \frac{1}{\tau_{ref}} \left(\frac{d}{d_0}\right)^4}{n \cdot \frac{1}{\tau_{ref}} \left(\frac{d}{d_0}\right)^4 + \sum k_i} = \frac{1}{1 + \frac{1}{n} \left(\frac{d}{d_0}\right)^4}$$

Under all the above assumptions, the ratio of the energy transfer rates of a multilayer graphene to a monolayer graphene is distance-independent.

$$\frac{k_{GET_{bilayer}}}{k_{GET_{monolayer}}} = \frac{k_{GET} + k_{GET}}{k_{GET}} = 2$$

$$\frac{k_{GET_{trilayer}}}{k_{GET_{monolayer}}} = \frac{k_{GET} + k_{GET} + k_{GET}}{k_{GET}} = 3$$

We tested the model experimentally with the help of single-molecule fluorescence measurements with both bilayer and trilayer graphene, and we checked the fluorescence quenching dependency by studying a few hundred single emitters placed at different distances from the multilayer graphene using DNA origami nanostructures. The results we obtained are in good agreement with our model. Namely, as the d_0 value increases with the number of layers, the working range also increases. Additional graphene layers forming bilayer and trilayer increase the active operating distance range of GET up to 50 – 60 nm, compared to about 40 nm for monolayer graphene.

The energy transfer efficiency η from an emitter to graphene can also be calculated from:

$$\eta = 1 - \frac{\tau_G}{\tau_{ref}}$$

such that the energy transfer rate therefore equals to:

$$k_{GET} = \frac{\eta}{\tau_G} = \frac{1}{\tau_G} - \frac{1}{\tau_{ref}}$$

where τ_G is the fluorescence lifetime of a dye molecule measured in the presence of graphene, and τ_{ref} is the fluorescence lifetime of the reference sample measured on glass (mean value averaged from the reference measurements of all DNA origami nanostructures on glass), and equals to:

3.27 ± 0.12 ns for ATTO542,

3.81 ± 0.15 ns for ATTO647N,

2.70 ± 0.12 ns for Cy3B.

Combining the above equations, we can also represent the fluorescence lifetime of an emitter in the function of its distance from graphene:

$$\tau_G = \tau_{ref} \cdot \left(\frac{1}{1 + \frac{1}{n}\left(\frac{d}{d_0}\right)^4} \right)$$

3.2. Characterization of monolayer and multilayer graphene.

3.2.1. Raman imaging

In this section, we divided the results into two parts. In the first subsection (Figure S1-S3), we present the two-dimensional Raman intensity maps that were recorded for various graphene samples: monolayer graphene (Figure S1a-c), bilayer graphene prepared using two-step layer-by-layer procedure involving two monolayers (Figure S2a-c), and bilayer graphene grown via chemical vapor deposition (CVD) (Figure S3a-c). Furthermore, we provide the exemplary Raman spectra for all samples (Figure S1d, S2d, S3d). The presented spectra were registered in the regions of the graphene surface that are marked with green spots on the “2D-to-G ratio” maps. These maps are particularly informative as the position of the G peak and the spectral features of the 2D band indicate the number of graphene layers. As expected, the monolayer graphene yields the highest uniformity. Conversely, there exists a notable contrast between the two variants of bilayer graphene. In both scenarios, the bilayer samples are comprised of a blend of two domains: monolayer and bilayer graphene. However, layer-by-layer graphene offers significantly larger regions where the bilayer domain dominates, while the "CVD-grown" sample consists predominantly of monolayer graphene with sporadically dispersed islands of bilayer graphene, oriented randomly.

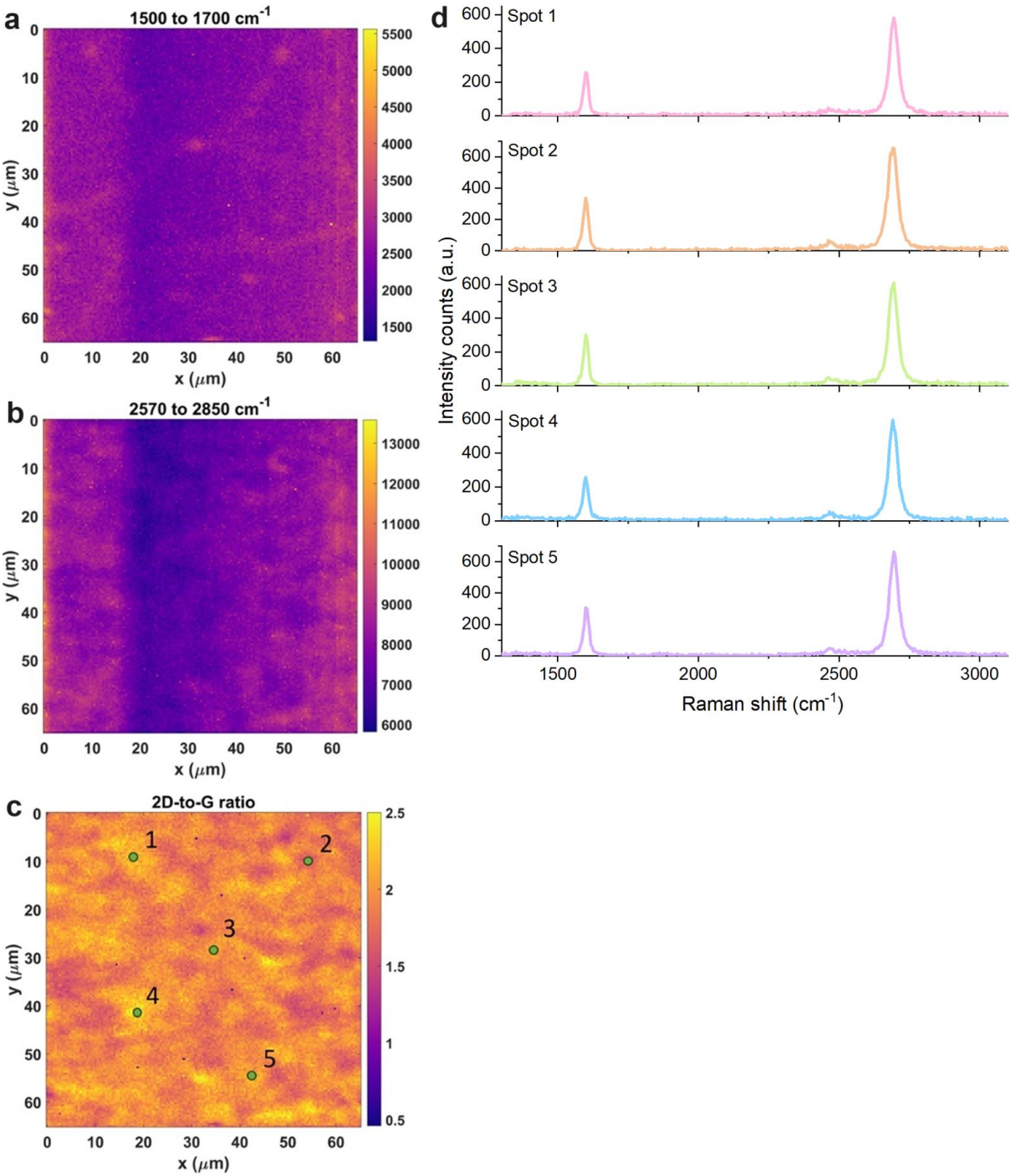

Figure S1. Two-dimensional Raman maps (65 × 65 μm) of monolayer graphene showing the intensity of the 2D peak (a), G peak (b) and the 2D to G ratio (c). The exemplary Raman spectra (d) were collected from the points on the graphene surface marked by green spots in Figure S1c.

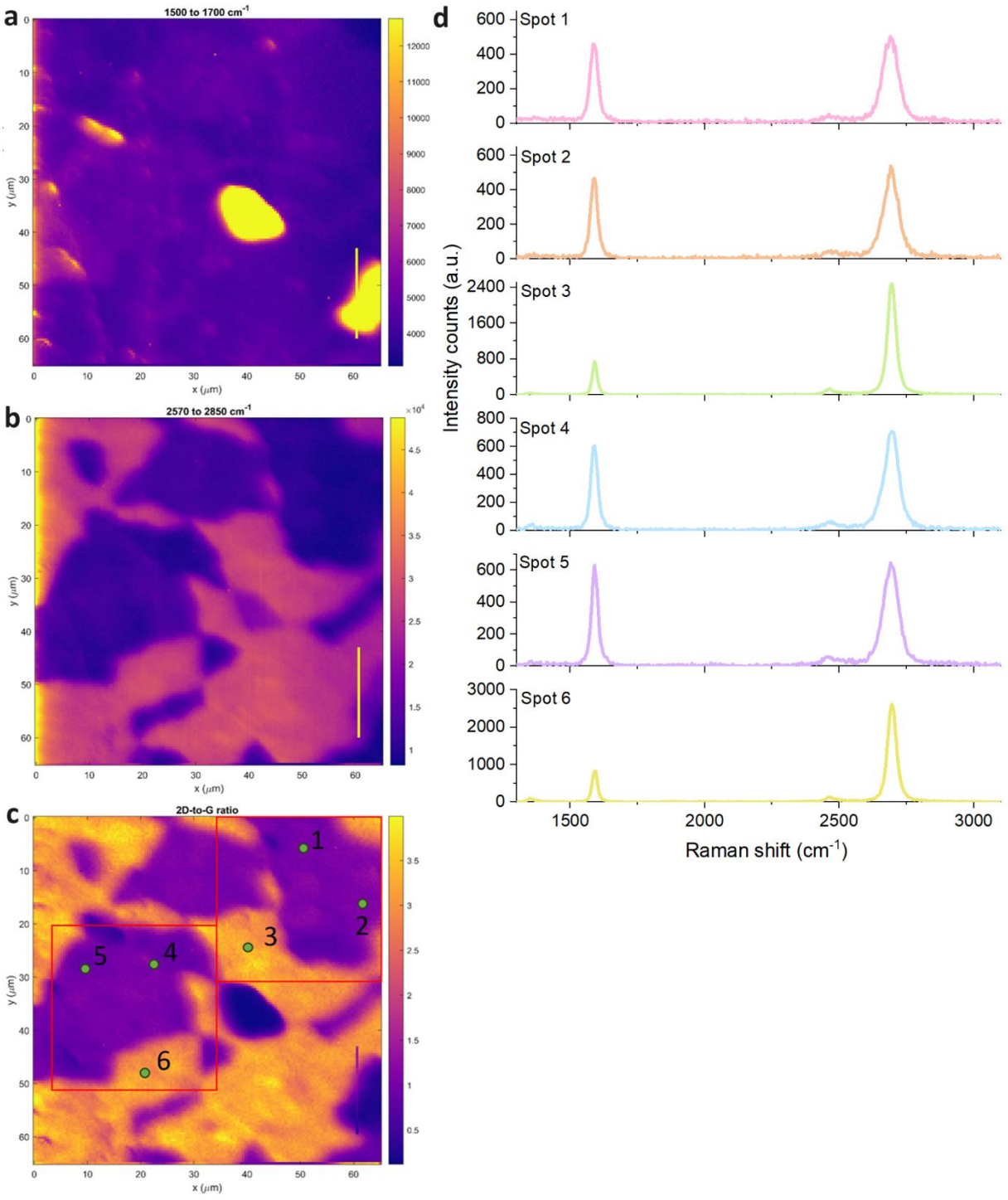

Figure S2. Two-dimensional Raman maps (65 × 65 μm) of bilayer (layer-by-layer) graphene showing the intensity of the 2D peak (a), G peak (b) and the 2D to G ratio (c). The exemplary Raman spectra (d) were collected from the points on the graphene surface marked by green spots in Figure S2c.

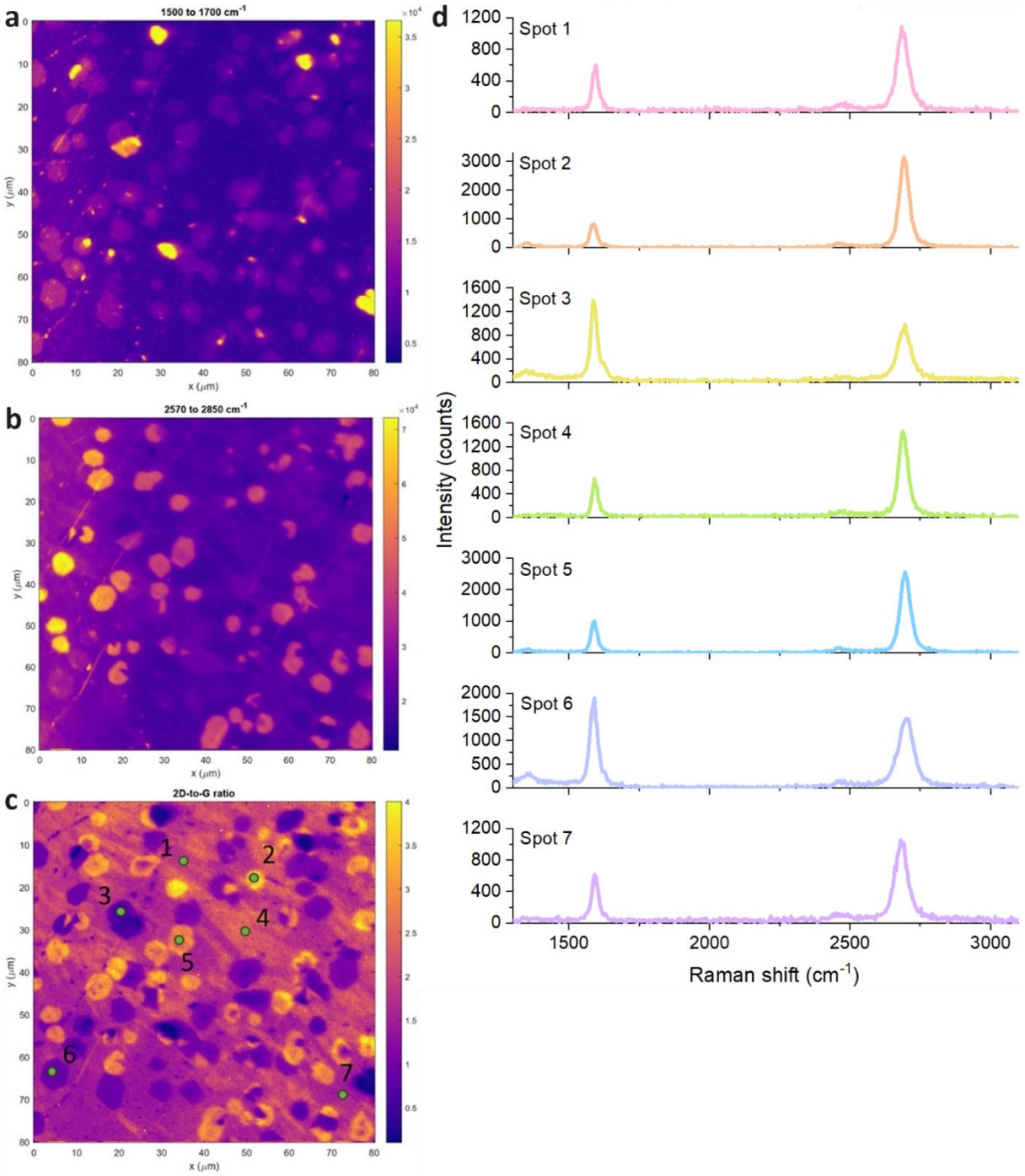

Figure S3. Two-dimensional Raman maps (80 × 80 µm) of CVD-grown bilayer graphene showing the intensity of the 2D peak (a), G peak (b) and the 2D to G ratio (c). The exemplary Raman spectra (d) were collected from the points on the graphene surface marked by green spots in Figure S3c.

For the second part of the Raman measurements, we prepared the bilayer graphene sample (layer-by-layer) in a way that enabled the collection of the Raman spectra of monolayer and bilayer graphene from the same sample (Figure S4b and S4c). We registered Raman intensity

maps (60 × 60 μm) of both regions and presented the exemplary Raman spectra (Figure S4b and S4c). We compared them with the spectra recorder for CVD-grown bilayer graphene (Figure S4d). The results are consistent with the above-presented Raman spectra proving higher homogeneity of the layer-by-layer bilayer graphene. However, we additionally confirmed the quality and quantity of graphene layers, of the same samples, by scanning electron microscopy imaging.

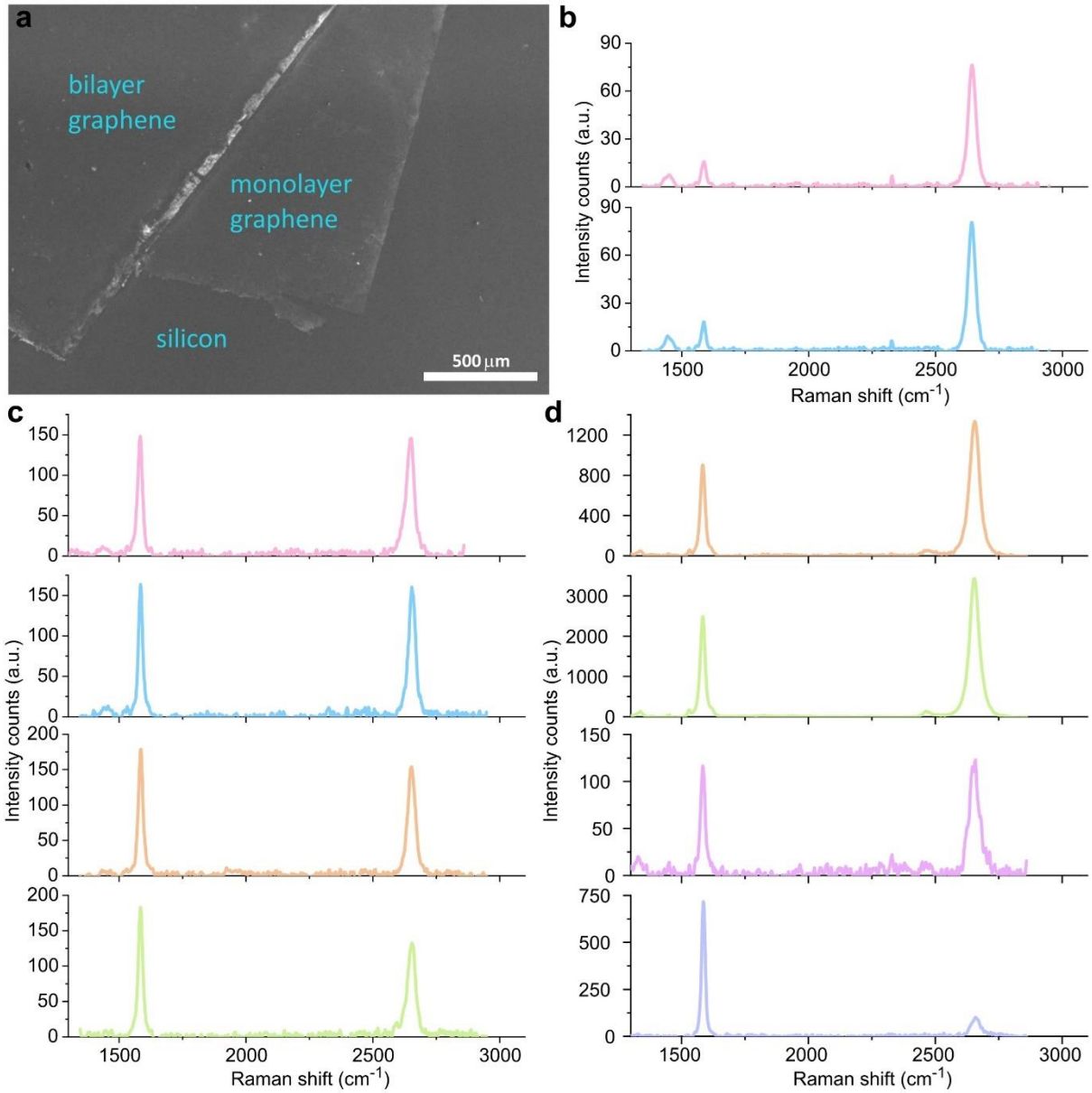

Figure S4. (a) SEM image of multilayer graphene substrate prepared layer-by-layer with marked regions of mono- and bilayer graphene, and silicon. Exemplary Raman spectra registered for the region of monolayer (b) and bilayer (c) graphene of the same sample. (d) Exemplary Raman spectra of CVD-grown bilayer graphene (SEM image not shown).

3.2.2. SEM imaging

The same samples that we checked by Raman microscopy (Figure S4), were also imaged using SEM (Figure S5). The findings align with the data acquired through Raman imaging, indicating that all examined samples exhibit exceptional quality with no visible defects or impurities. Notably, CVD-grown bilayer graphene is much more heterogeneous compared to the bilayer graphene prepared using our protocol.

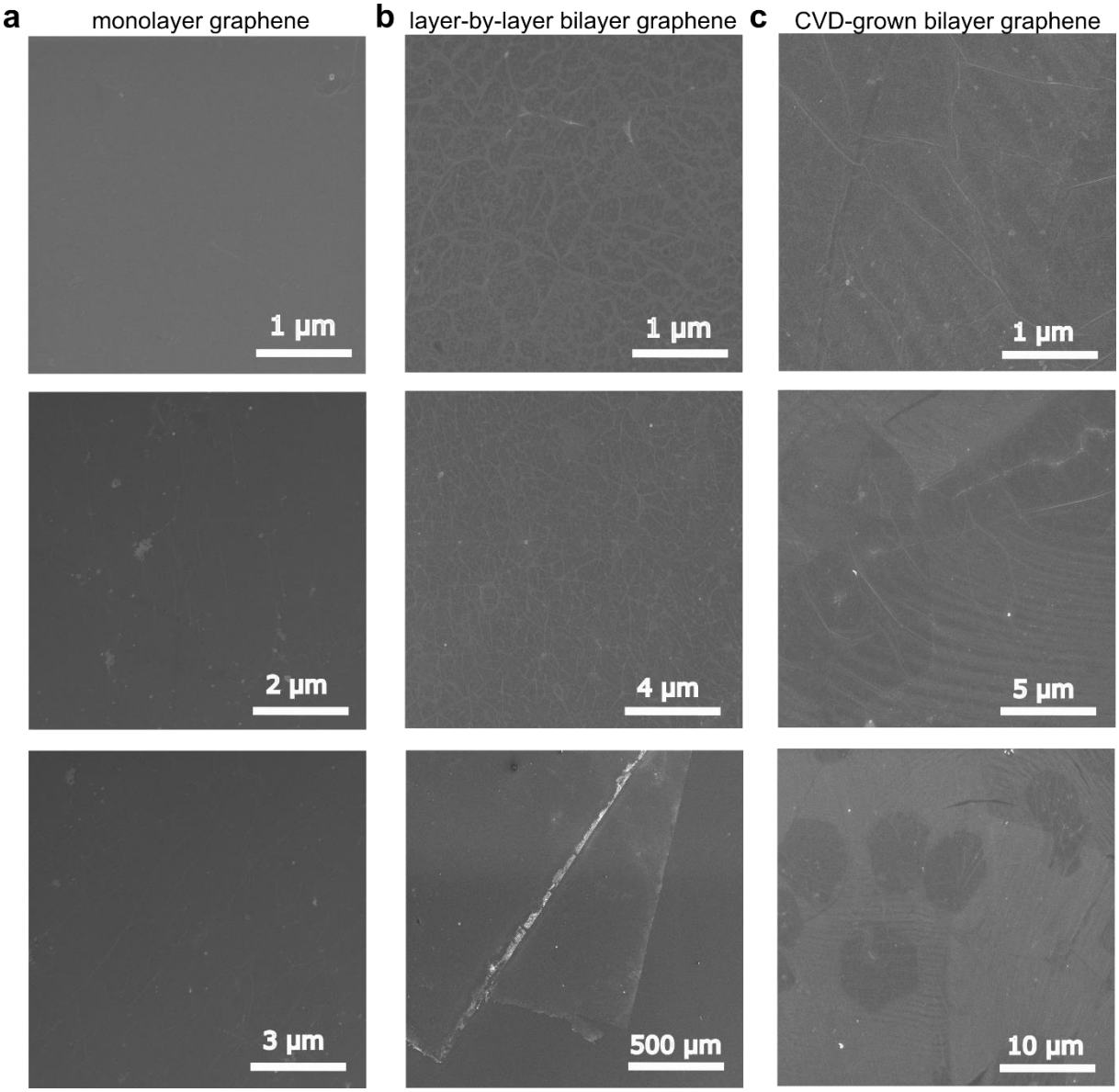

Figure S5. SEM images of monolayer graphene (a), bilayer (layer-by-layer) graphene (b) and CVD-grown bilayer graphene (c) at different magnifications.

3.3. Distance dependence of GET for mono- and multilayer graphene

All measurements for this part were carried out on the confocal setup (SI chapter 2.1) with a pulsed interleaved laser excitation of 532 nm and 639 nm. We used pillar-shaped DNA origami nanostructures labeled with two dye molecules, ATTO542 and ATTO647N at various heights ranging from 12 to 53 nm. We used the following ten combinations of heights/distances from graphene (ATTO542, ATTO647N): (12 nm, 24 nm), (16 nm, 16 nm), (16 nm, 24 nm), (16 nm, 30 nm), (24 nm, 16 nm), (24 nm, 30 nm), (24 nm, 40 nm) (30 nm, 53 nm), (40 nm, 24 nm), (53 nm, 30 nm). At first, we performed reference measurements on glass (Figure S6). Each DNA origami nanostructure was immobilized on neutravidin–biotinylated BSA glass coverslips using biotin modification at the base of the structure. We did not observe any fluorescence lifetime variations between the samples measured on glass, therefore we present combined data from 5 samples (1452 dye molecules) in Figure S6. The histograms with the Gaussian fit of the fluorescence lifetime values obtained for dyes ATTO542 and ATTO647N are depicted in Figure S6a, and the corresponding scatter plot of colocalized dye molecules in Figure S6b. While the examples of fluorescence decays of green (green) and red (magenta) dye molecules positioned in DNA origami nanostructures immobilized on glass fitted with the monoexponential function, with the fluorescence lifetime of ATTO542 and ATTO647N equal to 3.19 ns and 3.83 ns, respectively, are shown in Figure S6c.

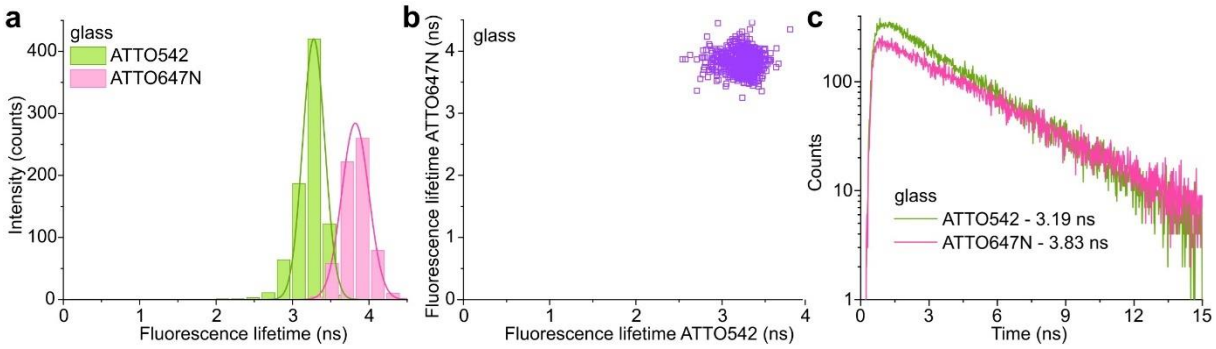

Figure S6. Reference measurements of the fluorescence lifetime of ATTO542 and ATTO647N dye molecules in the pillar-shaped DNA origami nanostructures immobilized on glass (combined data from 5 samples, 1452 dye molecules positioned at various heights). (a) Histograms fitted with a Gaussian function of the fluorescence lifetime (a), and the corresponding scatter plot of colocalized dye molecules. The mean fluorescence lifetime of ATTO542 ( ) equals 3.27 ± 0.12 ns, and 3.81 ± 0.15 ns for ATTO647N ( ). (c) Exemplary fluorescence decays of colocalized green (green) and red (magenta) dye molecules positioned

in DNA origami nanostructures immobilized on glass fitted with the monoexponential function. The fluorescence lifetime of ATTO542 and ATTO647N is equal to 3.19 ns and 3.83 ns, respectively.

To gain a better insight into the phenomenon of fluorescence quenching on bilayer and trilayer graphene, we expanded the range of the distances between the emitters and graphene substrates (monolayer, bilayer and trilayers) and conducted single-molecule studies for ten various DNA origami nanostructures (mentioned above). The results presented on histograms with a Gaussian function fit and the corresponding scatter plots are presented in Figure S7. Standard deviations of the fluorescence lifetime distributions presented in Figure S7 for all measured samples mainly stem from the heterogeneity of the graphene surface, likely related to the presence of defects, wrinkles, and holes. To a lesser extent it is influenced by the uncertainty of the fluorescence lifetime/decay fit of each single dye molecule, for which the standard deviation is several times smaller than the one obtained for the entire population.

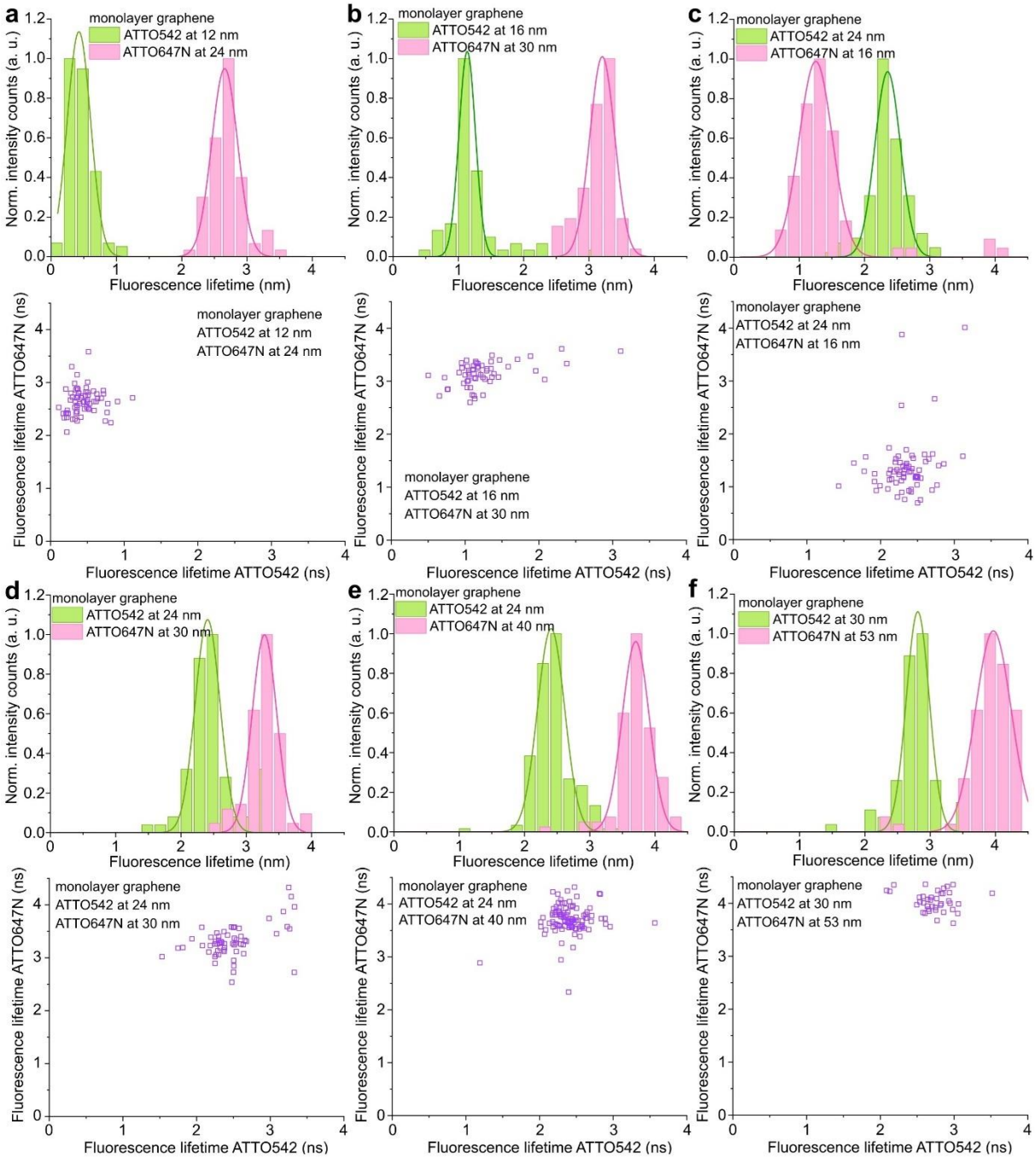
a
monolayer graphene
ATTO542 at 12 nm
ATTO647N at 24 nm
Norm. intensity counts (a. u.)
Fluorescence lifetime (nm)
b
monolayer graphene
ATTO542 at 16 nm
ATTO647N at 30 nm
c
monolayer graphene
ATTO542 at 24 nm
ATTO647N at 16 nm
Fluorescence lifetime ATTO647N (ns)
Fluorescence lifetime ATTO542 (ns)
d
monolayer graphene
ATTO542 at 24 nm
ATTO647N at 30 nm
e
monolayer graphene
ATTO542 at 24 nm
ATTO647N at 40 nm
f
monolayer graphene
ATTO542 at 30 nm
ATTO647N at 53 nm

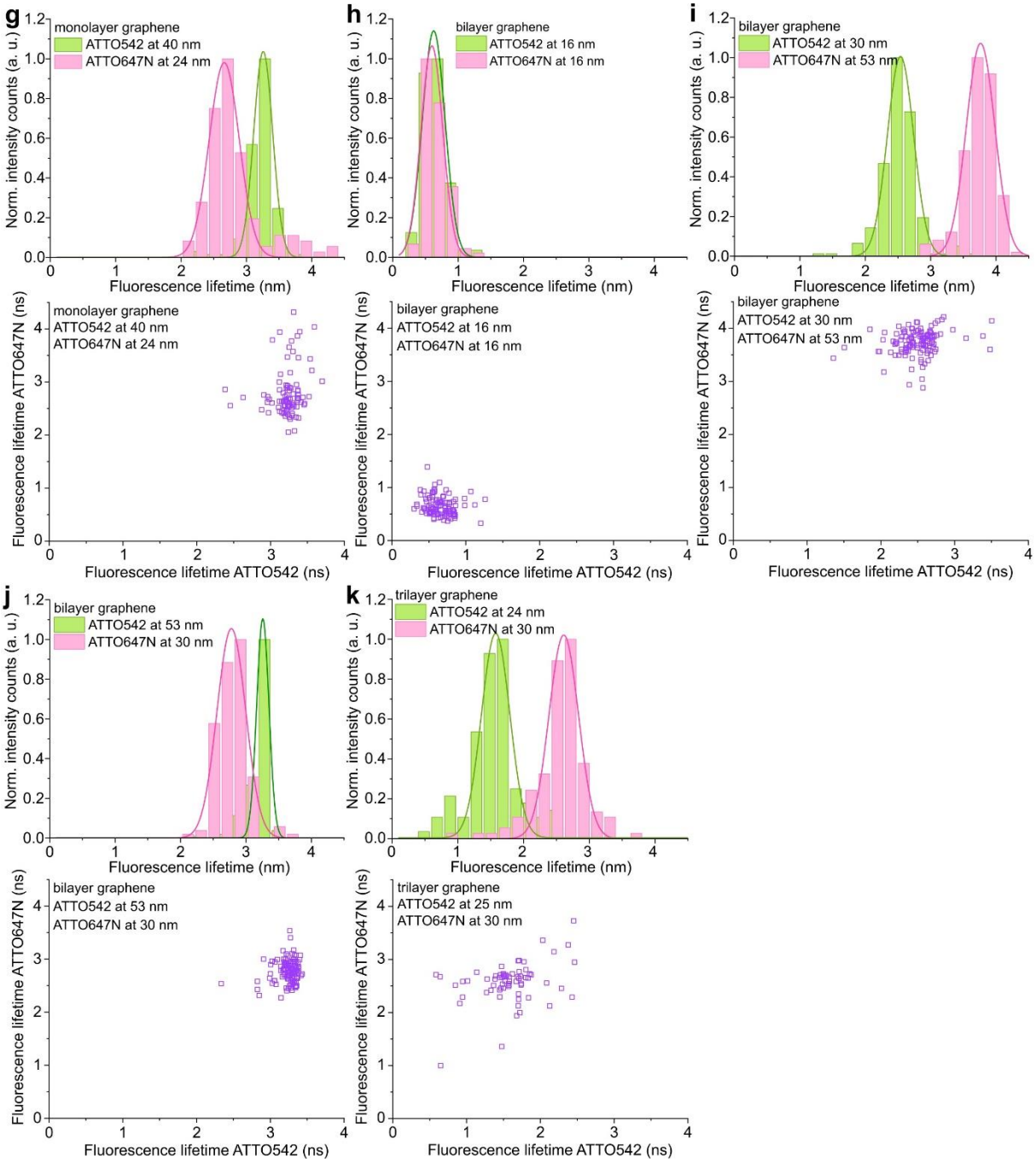

Figure S7. Histograms fitted with a Gaussian function of the fluorescence lifetime of colocalized dye molecules ATTO542 (green) and ATTO647N (magenta) positioned in DNA origami nanostructures immobilized on a monolayer (a – g), bilayer (h – j) and trilayer (k) graphene, together with the corresponding scatter plots of colocalized dye molecules. For the monolayer the dye molecules are positioned at: (a) 12 nm ( ) and 24 nm ( ), (b) 16 nm ( ) and 30 nm ( ), (c) 24 nm ( ) and 16 nm ( ), (d) 24 nm ( ) and 30 nm ( ), (e) 24 nm ( ) and 40 nm ( ), (f) 30 nm ( ) and 53nm ( ), (g) 40 nm ( ), and 24 nm ( ), for bilayer graphene: (h) 16 nm ( ) + 16 nm ( ), (i) 30 nm ( ) + 53 nm ( ), (j) 53 nm ( ), 30 nm ( ), whereas for trilayer graphene: (k) 24 nm ( ) and 30 nm ( ).

3.4. Dynamic assay for monolayer and bilayer GET

To stabilize Cy3B, a combination of ROXS and an oxygen scavenging system was used. The first buffer contained the aqueous solution of aged Trolox with PCA (PCA/Trolox12) and the second a 50× PCD (for measurements both buffers were mixed in a 1:50 ratio 50× PCD:Trolox/PCA12).[9,10]

We aimed to verify whether the introduction of more than one graphene layer to our system extends the dynamic range of GET. To this end, pillar-shaped DNA origami nanostructures equipped with the dynamic pointer (functionalized with Cy3B dye molecule) were immobilized on two substrates: monolayer and bilayer graphene. Among all of the possible heights at which we are able to study the dynamic assays, we chose 28 nm and 35 nm. Based on the curves calculated, for both heights, using the following equation:

$$\eta = \frac{1}{1 + \frac{1}{n}\left(\frac{d}{d_0}\right)^4}$$

We show that the pointer at 28 nm height leads to the highest difference between the monolayer and bilayer graphene. With the pointer at 35 nm, we can demonstrate that only with bilayer graphene we can resolve two binding states (Figure S8, S9).

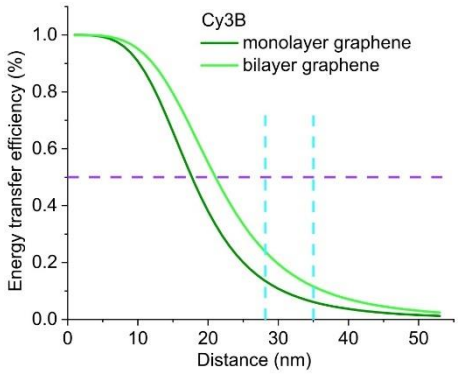

Figure S8. Graphene energy transfer efficiency as a function of distance calculated using the equation $\eta = \frac{1}{1+\frac{1}{n}\left(\frac{d}{d_0}\right)^4}$ for monolayer and bilayer graphene. Blue dashed lines indicate the heights of 28 nm and 35 nm selected for the studies of the dynamic assay systems, and purple dashed line indicates 50% of the energy transfer efficiency.

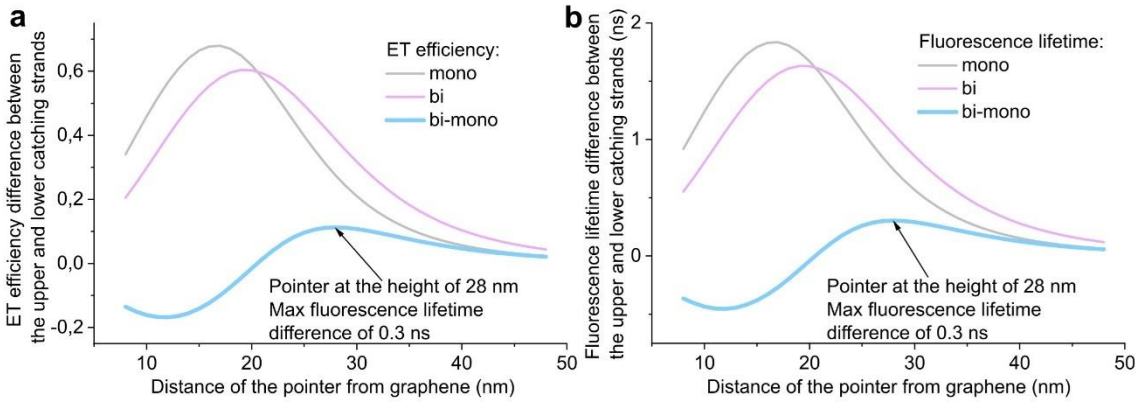

Figure S9. The graphene energy transfer efficiency ($\eta = \frac{1}{1+\frac{1}{n}\left(\frac{d}{d_0}\right)^4}$) difference between the upper and lower catching strands (a) and fluorescence lifetime ($\tau_G = \tau_{ref} \cdot \left(1 - \frac{1}{1+\frac{1}{n}\left(\frac{d}{d_0}\right)^4}\right)$) difference between the upper and lower catching strands (b) in the function of a distance calculated for monolayer (grey) and bilayer (magenta) graphene. The blue curves on both figures illustrate the difference between the GET of mono- and bilayer graphene (for lower and upper catching strands) showing that at 28 nm the difference between mono- and bilayer graphene is the highest yielding 0.3 ns difference of the fluorescence lifetime which corresponds to the maximum possible difference of the energy transfer efficiency value reaching 11 %.

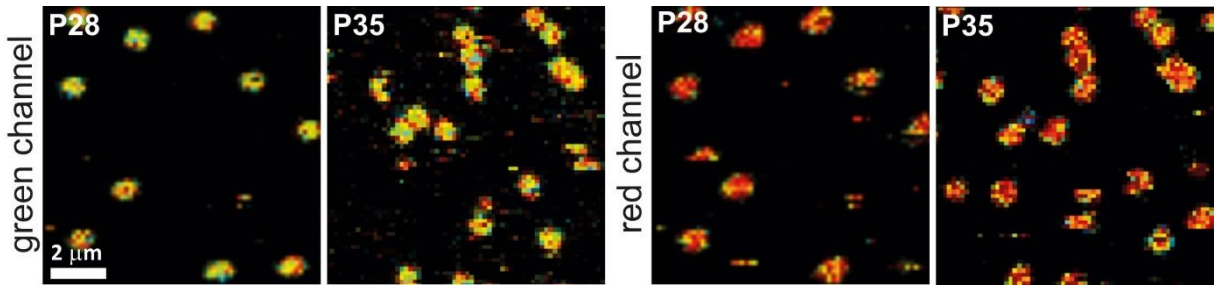

Figure S10. Reference measurements of fluorescence lifetime intensity maps (10 × 10 mm) obtained for the pointers positioned at the height of 28 nm (P28) or 35 nm (P35), labeled with a dye Cy3B (green channel, left panels) and ATTO647N (red channel, right panels) in the DNA origami nanostructures immobilized on glass.

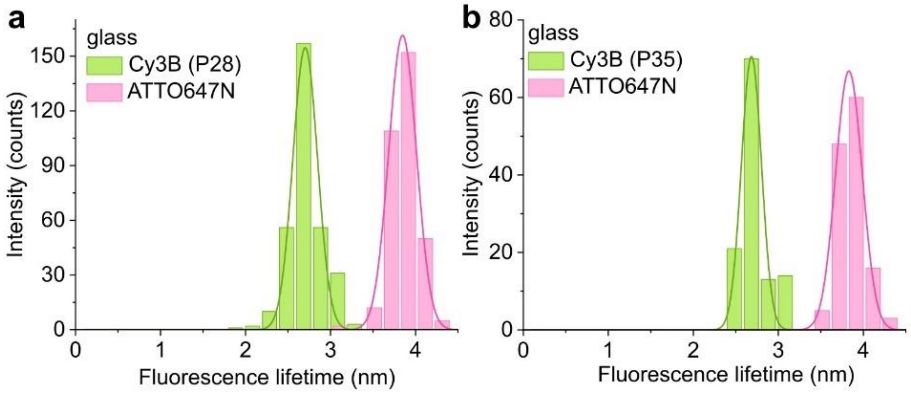

Figure S11. Histograms of the fluorescence lifetime of colocalized dye molecules Cy3B (green) and ATTO647N (magenta) positioned at 28 (a) and 35 nm (b) in the pillar-shaped DNA origami nanostructures immobilized on glass fitted with a Gaussian function. The fluorescence lifetime of Cy3B is equal to 2.70 ± 0.12 ns (a) and 2.69 ± 0.10 ns (b), whereas for ATTO647N equal to 3.85 ± 0.14 ns (a) and 3.83 ± 0.13 n (b).

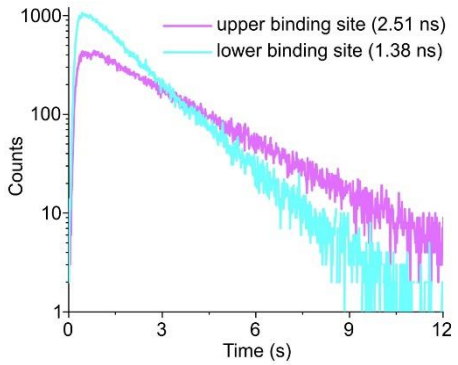

Figure S12. Fluorescence decays of the upper and the lower binding sites obtained for the pointer P28 immobilized on bilayer graphene presented in Figure 4a (fluorescence lifetime trace in pink).

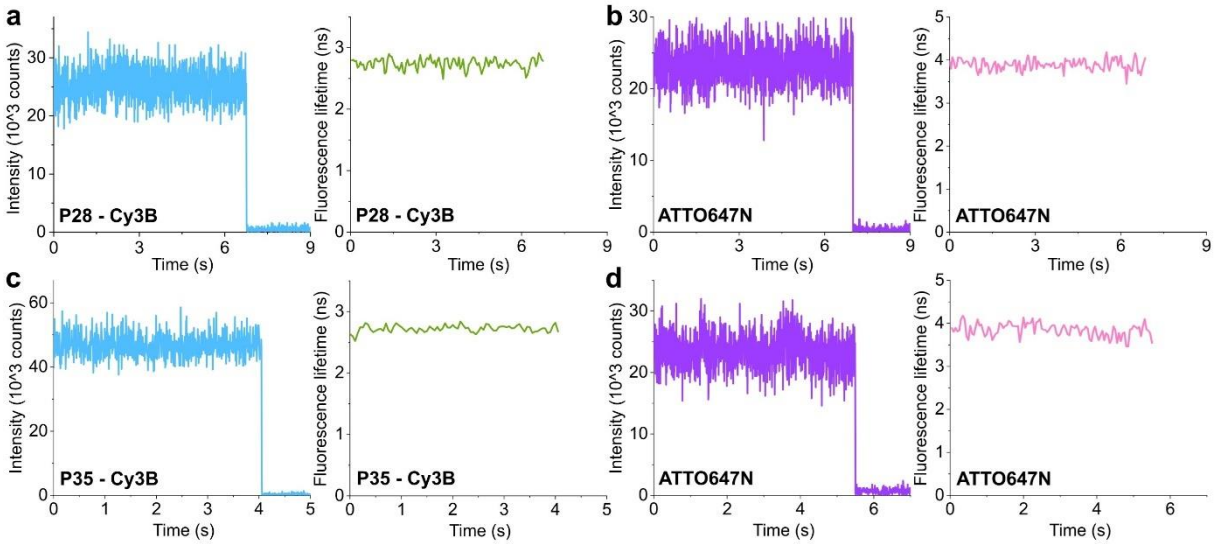

Figure S13. Examples of the fluorescence intensity (blue and violet) and the corresponding fluorescence lifetime (green and pink) time traces obtained from the pointer assay (ssDNA) positioned at the height of 28 nm (P28, a and c) and 35 nm (P35, b and d), labeled with a dye Cy3B (a – b), incorporated in the pillar-shaped DNA origami nanostructures immobilized on glass. Colocalization dye ATTO647N positioned at the height of 16 nm (c – d).

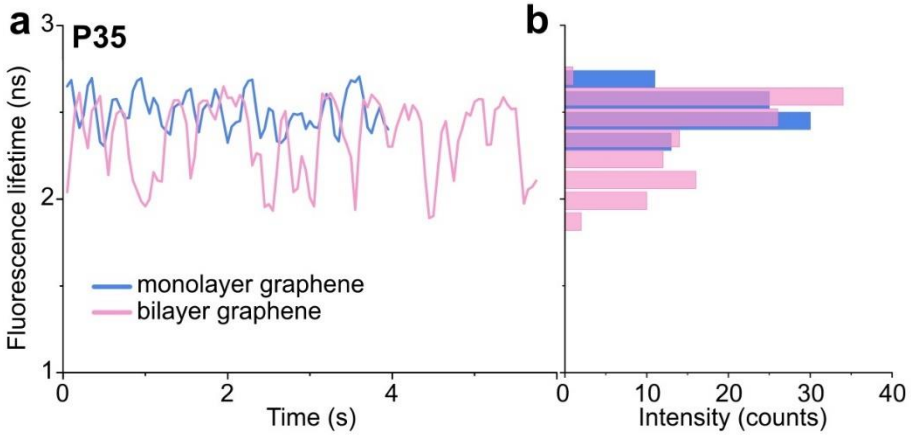

Figure S14. Examples of the fluorescence lifetime time traces (a) and the corresponding histograms (b) obtained for the pointer assay (ssDNA) positioned at the height of 35 nm labelled with a dye Cy3B, incorporated in the pillar-shaped DNA origami nanostructure immobilized on monolayer (blue) and bilayer (pink) graphene.

4. DNA sequences

Table S2. Core staples from the 5’ to the 3’ end for the pillar-shaped DNA origami structure.

Staple ID	Sequence (5’ to 3’)
P1	GAGAAGGCATCTGCAATGGGATAGGTCAAAAC
P2	AACCGTGTCATTGCAACGGTAATATATTTTAAATGAAAGGGT

Staple ID	Sequence (5’ to 3’)
P3	ATCGGTCAGATGATATTCACAAACCAAAAGA
P4	GCTGGCATAGCCACATTATTC
P5	CTGTATGGGATTACCGTTAGTATCA
P6	CCATAATGCCAGGCTATCAAGGCCGGAGACATCTA
P7	CTCATCGGGATTGAGTGAGCGAGTAACAACCCGTC
P8	TAGCCAGCTTTCATCCAAAAATAAACGT
P9	TAGCCTCAGAGCATACCCTGT
P10	AATACCCCAACATTCATCAAAAATAATTCGCGTCT
P11	GGCTAAAACTTCAGAAAAGTTTTGCGGGAGATAGAACC
P12	CCCGGTTGATAAAGCATGTCAATC
P13	ATCGATGCTGAGAGTCTACAAGGAGAGGGAACGCCAAAAGGA
P14	GACAATTACGCAGAGGCATTTTCGAG
P15	TAAGTTGGCATGATTAAAGAA
P16	CCAATGTTTAAGTACGGTGTCCAAC
P17	CGGAATAGAAAGGAATGCCTTGCTAAACAACTTTCAAC
P18	GAGTTAAAAGGGTAATTGAGCGCTAATATCAGAGGAACTGAACACC
P19	TTTAGCGATACCAACGCGTTA
P20	TTTTTGCGGATGCTCCTAAAATGTTTAGATGAATTTTGCAAAAGAAGTT
P21	AATAAAACGAACTATGACCCCACCAAGC
P22	AATATCGTTAAGAGAGCAAAGCGGATTGTGAAAAATCAGGTCTTT
P23	ATTACGAGATAAATGCCAGCTTTGAGGGGACGACGACAG
P24	ACAACGCCTGTAGCATTTACCGTATAGGAAG
P25	TTACCATTAGCAAGGCCTTGAATTAGAGCCAGCCCGACTTGAGC
P26	CAGCAGCGCCGCTTGTTTATCAGCTTCACGAAAAA
P27	CTTACGGAACAGTCAGGACGTTGGGAAGAAA
P28	AGCTCTTACCGAAGCCCAATA
P29	TATTACGAATAATAAACAAATCAGATATGCGT
P30	CACGGCAACAATCCTGATATACTT
P31	CATCGAGATAACGTCAAACATAAAAGAGCAAAAGAATT
P32	CAAGCCCAATAGGAACCACCCTCACCCGGAA
P33	CATTTCGCAAATGTCATCTGCGAACGAGAGATTCACAATGCC
P34	GGCGCAGACGGTCAATCATCGAGACCTGCTCCATGTGGT
P35	CAAACGGAATAGGAAACCGAGGAATAAGAAATTACAAG
P36	ACCAACAAACCAAAATTAACAATTTCATTTGAATTACCGAGG
P37	CATTTGAGATAACCCACGAAACAATG
P38	AGGACAGATGAACGGTGTAACATAAGGGAACCGAAGAAT
P39	TGGCTTTTTACCGTAGAATGGAAAGCG
P40	GTTAAAGGAAAGACAGCATCTGCCTATTTAAGAGGCAGGAGGTTTA
P41	AGTAGGTATATGCGTTATACA
P42	CGAACACCAAATAAAATAGCAGCCAAGTTTGCCTTTAGCGTCAGA
P43	GCGAAACAAAGTGTAAAACACATGGCCTCGATTGAACCA
P44	AAGAAAGCTTGATACCGCCACGCATACAGACCAGGCGCTGAC
P45	CTGAATATAGAACCAAATTATTTGCACGTAAAACAACGT
P46	AGACAGCAGAAACGAAAGAGGAAATAAATCGAGGTGACAGTTAAAT
P47	CGAGGGTACTTTTTCATGAACGGGGTCATAATGCCGAGCCACCACC
P48	TAAAGCCTCCAGTACCTCATAGTTAGCG
P49	AATATGCAACTACCATCATAGACCGGAACCGC
P50	AGAAATCGTTAGACTACCTTTTTAAGGCGTTCTGACCTTTTTGCA
P51	CTAAATCGGTCAGAATTAGCAAAATTAAGCAATAAAATAATA
P52	AAATCAGCTCATTTTTTAACCATTTTGTTAAAATTCGCATTA
P53	ATAGCGAGAGGCTATCATAACCAAATCCCAAAGAAAATTTCATCCTCAT
P54	GAACTGGCTCATTACAACTTTAATCATTCTTGAGATTACTTA

Staple ID	Sequence (5’ to 3’)
P55	ACGCGAGAGAAGGCCATGTAATTTAGGCCAGGCTTAATTGAGAATCGC
P56	TAATATCAAAGGCACCGCTTCTGGCACT
P57	TTTCCATGGCACCAACCTACGTCATACA
P58	AAGACAAATCAGCTGCTCATTCAGTCTGACCA
P59	CCGTAATCAGTAGCGACAGAATCTAATTATTCATTAAAAAGG
P60	CTGGCATTAGGAGAATAAAATGAAGAAACGATTTTTTGAGTA
P61	CGCGCCGCCACCAGAACAGAGCCATAAAGGTGGAA
P62	TAGCCCGGAATAGGTGTAAGGATAAGTGCCGTCGA
P63	AAGGCTCCAAAAGGAGCCTTTATATTTTTTCACGTGCTACAGTCACCCT
P64	CAAAATCACCGGAACCAGAGCCAGATTTTGTCACAATCACAC
P65	AATTGTGTCGAAATCCGCGGCACACAACGGAGATTTGTATCA
P66	CCTCGTCTTTCCACCACCGGAACCGCCTCCCTCA
P67	CCGTGTGATAAATAACCTCCGGCTGATG
P68	CCCAGCTACAATGACAGCATTTGAGGCAAGTTGAGAAATGAA
P69	TATTTAAATTGCAGGAAGATTG
P70	AAGGGATATTCATTACCGTAATCTATAGGCT
P71	ACCAGACCGGATTAATTCGAGC
P72	AAGGCCTGTTTAGTATCATGTTAGCTACCTC
P73	AGCAACAAAGTCAGAAATAATATCCAATAATCGGCTCAGGGA
P74	TGAGTAAAGGATAAGTTTAGCTATATCATAGACCATTAGATA
P75	GAGTCTGGATTTGTTATAATTACTACATACACCAC
P76	TTCGGTCCCATCGCATAGTTGCGCCGACATGCTTTCGAGGTG
P77	CGTGTCAAATCACCATCTAGGTAATAGATTT
P78	GGAACCATACAGGCAAGGCAAATCAAAAAGACGTAGTAGCAT
P79	ATTTGGAAGTTTCATGCCTCAACATGTTTTA
P80	AATTTCTTAAACCCGCTTAATTGTATCGTTGCGGGCGATATA
P81	GAGCATTTATCCTGAATCAAACGTGACTCCT
P82	TTATAAGGGTATGGAATAATTCATCAATATA
P83	TAACGACATTTTTACCAGCGCCAAAGAAAGTTACCAGAACCCAAA
P84	AAAGATTACAGAACGGGAGAAGGAAACGTCACCAATGAAACCA
P85	GCTGTAGTTAGAGCTTAATTG
P86	AGTTTCCAACATTATTACATTATAC
P87	GGGATATTGACGTAGCAATAGCTAAGATAGC
P88	AACAAGAGCCTAATGCAGAACGCGC
P89	AGTTTATTGTCCATATAACAGTTGATTC
P90	TATTGAAAGGAATTGAGGTAG
P91	AATAGAAAAAAATAAACGTCTGAGAGGAATATAAGAGCAACACTATGAT
P92	TCGTGCCGGAGTCAATAGTGAATTTGCAGAT
P93	TTAGTTTGAGTGCCCGAGAAATAAAGAAATTGCGTAGAGATA
P94	TTGGTAGAACATTTAATTAAGCAAC
P95	TAACATCCAATAAATGCAAAGGTGGCATCAACATTATGAAAG
P96	TAAGTTTACACTGAGTTTCGT
P97	AGAACTTAGCCTAATTATCCCAAGCCCCCTTATTAGCGTTTGCCA
P98	ACCGCCACCCTCAGAACCCGTACTCTAGGGA
P99	TTAGCCCTGACGAGAAACACCAGAAATTGGGGTGAATTATTTTAA
P100	ATAAAGTCTTTCCTTATCACT
P101	ATTTCCTGATTATCAGATGATGGCTTTAAAAAGACGCTAAAA
P102	ACATAAGTAGAAAAATCAAGAAGCAAAAGAAGATGTCAT
P103	TTCATCGGCATTTTCGGTCATATCAAAA
P104	GAACCGCCACCCTCCATATCATACC
P105	ACTAATGCCACTACGAATAAA
P106	CAAGCCGCCCAATAGCAAGTAAACAGCCATATTATTTTGCCATAAC

Staple ID	Sequence (5’ to 3’)
P107	TGAAAATCCGGTCAATAACCTAAATTTTAGCCTTT
P108	CCTCGTTTACCAGAAACCAAA
P109	CAAATTATTCATTTCAATTACCTGAGTA
P110	ATTTCAACCAAAAATTCTACTAATAGTTAGTTTCATTTGGGGCGCGAGC
P111	AGGCTTGCGAGACTCCTCAAGAGAAAAGTATTCGGAAC
P112	AATATTCATTGAATCCATGCTGGATAGCGTCCAAT
P113	CTAGTCAGTTGGCAAATCAACAGTCTTTAGGTAGATAACAAA
P114	TATGACTTTATACATTTTTTTTTAATGGAAACAGTACACCGT
P115	ACTAAAGAGCAACGTGAAAATCTCCACCCACAACTAAAGGAA
P116	TTGCGAATAATATTTACAGCGGAGTGAGGTAAAATTTTGAGG
P117	CCGACTTGTTGCTAAAATTTATTTAGTTCGCGAGAGTCGTCTTTCCAGA
P118	ATTGTTATCTGAGAAGAAACCAGGCAAAGCGCCATTCGTAGA
P119	AGTACCGCATTCCACAACATGTTCAGCCTTAAGGTAAAGTAATTC
P120	AAACTCACAGGAACGGTACGCCAGTAAAGGGGGTGAGGAACC
P121	CGCTTTCCAGTTAGCTGTTTAAAGAACGT
P122	GGCGAAGCACCGTAATAACGCCAGGGTTTTCCCAGTCATGGG
P123	TTTACCAGTCCCGGCCTGCAGCCCACTACGGGCGCACCAGCT
P124	GGCAACACCAGGGTCTAATGAGTGAGCTCACAACAATAGGGT
P125	GAAGGAGCGGAATTATCATCATATATCATTTACATAGCACAA
P126	CGCGCTACAGAGTAATAAAAGGGACATTCTGATAGAACTTAG
P127	GTAATTAATTTAGAATCTGGGAAGGGCGATCGGTGCGGCAAA
P128	GGATGTGGTTTGCCCCAGCAG
P129	GCCAGCAGTTGGGCGCAAATCAGGTTTCTTGCCCTGCGTGGT
P130	TATCAGCAACCGCAAGAATGCCAATGAGCCTGAGGATCTATC
P131	GAGAACAATATACAAAATCGCGCAGAGGCGATTCGACAAATCCTTTAAC
P132	GTAAAACGACGGCCCATCACCCAAATCAGCGC
P133	ACGGGCCGATAATCCTGAGAAGTGTTTTTATGGAGCTAACCG
P134	TGCTAAATCGGGGAGCCCCCGATTTAGAGCTAGCAGAACATT
P135	ACGCGGTCCGTTTTTGGGTAAGTGA
P136	GCGTCCACTATTCCTGTGTGAAATGCTCACTGCC
P137	CGTACTATGGTAACCACTAGTCTTTAATGCGCGAACTGAATC
P138	AGAATTTTAGAGGAAAACAATATTACCGCCAGCTGCTCATTT
P139	TTGGGCGGCTGATTTCGGCAAAATCCCT
P140	TGGTGGTTGTTCCAGTTTGGAACA
P141	AGTCGCCTGATACTTGCATAACAGAATACGTGGCACAGCTGA
P142	TGCTGATTGCCGTTGTCATAAACATCGGGCGG
P143	TGAGTGTTCCGAAAGCCCTTCACCGCCTAGGCGGTATTA
P144	TGAGCAAATTTATACAGGAATAACATCACTTGCCTGAGTCTT
P145	CCTGCGCTGGGTGGCGAGAAAGGAAGGGAAGGAGCGGGGCCG
P146	CGTACAGGCCCCCTAACCGTCCCCGGGTACCGAGCGTTC
P147	TTTAGATTCACCAGTCACACGACCGGCGCGTGCTTTCCCAGA
P148	CCCCGCTAGGGCAACAGCTGGCGAAAGGGGGATGTGCTTATT
P149	TCACAGCGTACTCCGTGGTGAAGGGATAGCTAAGAGACGAGG
P150	TGCGTGTTCAGGTTGTGTACATCG
P151	AGGGAGCCGCCACGGGAACGGATAGGCGAAAGCATCAGCACTCTG
P152	AAGAAAGCGCTGAACCTCAAATATTCTAAAGGAAAGCGTTCA
P153	AGCGCAGCTCCAACCGTAATCATGGTCACGGGAAACCT
P154	CCTCATCACCCCAGCAGGCCTCTTCGCTATTACGCCAGTGCC
P155	GTCGCGTGCCTTCGAATTGTCAAAG
P156	TTCGGGGTTTCTGCCAGGCCTGTGACGATCC
P157	AGAGAAAATCCAGAGAGTTGCAGCAAATC
P158	TGCCATCCCACGCAGGCAGTTCCTCATTGCCGTTTTAAACGA

Staple ID	Sequence (5’ to 3’)
P159	GCCCGAGTACGAGCCGGAAGC
P160	GAGGCCAAGCTTTGAATACCAAGTACGGATTACCTTTTCAAA
P161	ACGTAAGAATTCGTTCTTAGAAGAACTCAAACTATCGGATAA
P162	TAAAACCGTTAAAGAGTCTGTCCATCCAGAAACCACACAATC
P163	ACGAGCGGCGCGGTCAGGCAAGGCGATTAAGTTGGGTAAAAC
P164	TTTTCCAGCATCAGCGGGGCTAAAGAACCTCGTAGCACGCCA
P165	CAAAGCACTAGATAGCTCCATTCAGGCTGCGCAACTGTCTTG
P166	ATTGCGTTGCTGTTATCCGCTCACAATTCCAAACTCACTTGCGTA
P167	GAGAGATAGACTTTACGGCATCAGA
P168	TGACCGCGCCTTAATTTACAATATTTTTGAATGGCTATCACA
P169	CCTAATTTAACAAACCCTCAATCAATATCTGATTCGCTAATC
P170	TTAACTCGGAATTAGAGTAAATCAATATATGTGAGTGATTCT
P171	ATGAAGGGTAAAGTTCACGGTGCGGCCATGCCGGTCGCCATG
P172	ACATAAAGCCCTTACACTGGTCGGGTTAAATTTGT
P173	AAATGCGGAAACATCGGTTTTCAGGTTTAACGTCAGATTAAC
P174	GTCGCAGAAAAACTTAAATTTGCC
P175	GAATTCGTCTCGTCGCTGGGTCTGCAATCCATTGCAACACGG
P176	GCGAAAATCCCGTAAAAAAAGCCGTGGTGCTCATACCGGCGTCCG
P177	CTTGTAGAACGTCAGCGGCTGATTGCAGAGTTTTTCGACGTT
P178	TCATACATTTAATACCGATAGCCCTAAAACATCGAACGTAAC
P179	TACGGCTGGAGGTGCGCACTCGTCACTGTTTGCTCCCGGCAA
P180	AAATGACGCTAAATGGATTATTTACATTGGCGAATACCTGGA
P181	AACAACAGGAAGCACGTCCTTGCTGGTAATATCCAGAAACGC
P182	TGCATTAATGAGCGGTCCACGCTCACTGCGCCACGTGCCAGC
P183	ACCTGACGGGGAAAGCCGGCGAACCAAGTGTCTGCGCGTTGC
P184	CCAGCCTCCGATCCTCATGCCGGA
P185	GCTGGTCTGGTCAGGAGCCGGAATCCGCCGTGAACAGTGCCA
P186	GCGAATCAGTGAGGCCACCGAGTAGTAGCAACTGAGAGTTGA
P187	GGCCAACGCGCGGGGAGGGCCCTGTGTTTGA
P188	AGCTTTCAGAGGTGGCGATGGCCAGCGGGAAT
P189	ATTAGCGGGGTTTTGCTCAGTACCAGGCTGACAACAAGCTG
P190	TGCCCGTATAAACAGTGTGCCTTCTGGTAA
P191	AGAAAACGAGAATGACCATAAATCTACGCCCCTCAAATGCTTTA
P192	ATAACTATATGTAAATGCTTAGGATATAAT
P193	AGGAATCATTACCGCGTTTTTATAAGTACC
P194	GATTAGAGAGTACCTTAACTCCAACAGG
P195	CCTTAAATCAAGATTAGCGGGAGGCTCAAC
P196	GCATGTAGAAACCAATCCATCCTAGTCCTG

Table S3. Biotin-modified staples from the 5’ to the 3’ end for the pillar-shaped DNA origami structure.

Sequence (5’ to 3’)	Function	Replace
Biotin-AGAAAACGAGAATGACCATAAATCTACGCCCCTCAAATGCTTTA	Immobilization on glass	P189
Biotin-ATTAGCGGGGTTTTGCTCAGTACCAGGCTGACAACAAGCTG	Immobilization on glass	P190
Biotin-GCATGTAGAAACCAATCCATCCTAGTCCTG	Immobilization on glass	P191
Biotin-GATTAGAGAGTACCTTAACTCCAACAGG	Immobilization on glass	P192
Biotin-TGCCCGTATAAACAGTGTGCCTTCTGGTAA	Immobilization on glass	P193

Sequence (5’ to 3’)	Function	Replace
Biotin-CCTTAAATCAAGATTAGCGGGAGGCTCAAC	Immobilization on glass	P194
Biotin-AGGAATCATTACCGCGTTTTTATAAGTACC	Immobilization on glass	P195
Biotin-ATAACTATATGTAAATGCTTAGGATATAAT	Immobilization on glass	P196

Table S4. Staples from the 5’ to the 3’ end for the pillar-shaped DNA origami structure with extensions for immobilization on graphene.

Sequence (5’ to 3’)	Function	Replace
ATATTTCCTCTACCACCTACATCACTAATTAGCGGGGTTTTGCTCAGTACCAGGCTGACAACAAGCTG	Immobilization on graphene	P189
ATATTTCCTCTACCACCTACATCACTAAGAAAACGAGAATGACCATAAATCTACGCCCCTCAAATGCTTTTA	Immobilization on graphene	P190
ATATTTCCTCTACCACCTACATCACTAATAACTATATGTAAATGCTTAGGATATAAT	Immobilization on graphene	P191
ATATTTCCTCTACCACCTACATCACTAGCATGTAGAAACCAATCCATCCTAGTCCTG	Immobilization on graphene	P192
ATATTTCCTCTACCACCTACATCACTATGCCCGTATAAACAGTGTGCCTTCTGGTAA	Immobilization on graphene	P193
ATATTTCCTCTACCACCTACATCACTAAGGAATCATTACCGCGTTTTTATAAGTACC	Immobilization on graphene	P194
ATATTTCCTCTACCACCTACATCACTAGATTAGAGAGTACCTTAACTCCAACAGG	Immobilization on graphene	P195
ATATTTCCTCTACCACCTACATCACTACCTTAAATCAAGATTAGCGGGAGGCTCAAC	Immobilization on graphene	P196

Table S5. Staples from the 5’ to the 3’ end for the pillar-shaped DNA origami structure for “Distance determination and distance scaling law for mono- and multilayer graphene”.

Sequence (5’ to 3’)	Function	Replace
AGACAGCAGAAACGAAAGAGGAAATAAATCGAGGTGACAGTTAAAT-**ATTO542**	Dye ATTO542 at 3’ (12 nm)	P46
AATATGCAACTACCATCATAGACCGGAACCGC-**ATTO542**	Dye ATTO542 at 3’ (16 nm)	P49
AATATGCAACTACCATCATAGACCGGAACCGC-**ATTO647N**	Dye ATTO647N at 3’ (16 nm)	P49
AAGGGATATTCATTACCGTAATCTATAGGCT-**ATTO542**	Dye ATTO542 at 3’ (24 nm)	P70
AAGGGATATTCATTACCGTAATCTATAGGCT-**ATTO647N**	Dye ATTO647N at 3’ (24 nm)	P70
ATTGTTATCTGAGAAGAAACCAGGCAAAGCGCCATTCGTAGA-**ATTO542**	Dye ATTO542 at 3’ (30 nm)	P118
ATTGTTATCTGAGAAGAAACCAGGCAAAGCGCCATTCGTAGA-**ATTO647N**	Dye ATTO647N at 3’ (30 nm)	P118
TAAAACCGTTAAAGAGTCTGTCCATCCAGAAACCACACAATC-**ATTO542**	Dye ATTO542 at 3’ (40 nm)	P162
TAAAACCGTTAAAGAGTCTGTCCATCCAGAAACCACACAATC-**ATTO647N**	Dye ATTO647N at 3’ (40 nm)	P162
ACGGGCCGATAATCCTGAGAAGTGTTTTTATGGAGCTAACCG- **ATTO542**	Dye ATTO542 at 3’ (53 nm)	P133

Sequence (5’ to 3’)	Function	Replace
ACGGGCCGATAATCCTGAGAAGTGTTTTTATGGAGCTAACCG-ATTO647N	Dye ATTO647N at 3’ (53 nm)	P133

Table S6. Staples from the 5’ to the 3’ end for the pillar-shaped DNA origami structure for “Dynamic assay for monolayer and bilayer GET”.

Sequence (5’ to 3’)	Function	Replace
Cy3B-ATTTACGGGCTTTTTTTTTTTTTATTGAAAGGAATTGAGGTAG	Pointer P28 at 5’	P90
CGTAAATTTTGATACATAAGTAGAAAAATCAAGAAGCAAAAGAAGATGTCAT	Low binding strand for P28	P102
CGTAAATTTTCTAGTCAGTTGGCAAATCAACAGTCTTTAGGTAGATAACAAA	High binding strand for P28	P113
Cy3B-ATTTACGGGCTTTTTTTTTTTTTCTAGTCAGTTGGCAAATCAACAGTCTTTAGGTAGATAACAAA	Pointer P35 at 5’	P113
CGTAAATTTTTATTGAAAGGAATTGAGGTAG	Low binding strand for P35	P90
CGTAAATTTTTAACAAACCCTCAATCAATATCTGATTCGCTAATC	High binding strand for P35	P169
TAAAACCGTTAAAGAGTCTGTCCATCCAGAAACCACACAATCCCTAATT	Exchange staple	P162
AATATGCAACTACCATCATAGACCGGAACCGC-ATTO647N	Reference dye ATTO647N at 3’ (16 nm)	P49

5. References.

1 S. Krause, E. Ploetz, J. Bohlen, P. Schuler, R. Yaadav, F. Selbach, F. Steiner, I. Kamińska and P. Tinnefeld, *ACS Nano*, 2021, **15**, 6430–6438.

2 P. C. Nickels, B. Wünsch, P. Holzmeister, W. Bae, L. M. Kneer, D. Grohmann, P. Tinnefeld and T. Liedl, *Science*, 2016, **354**, 305–307.

3 Y. Ke, S. M. Douglas, M. Liu, J. Sharma, A. Cheng, A. Leung, Y. Liu, W. M. Shih and H. Yan, *J Am Chem Soc*, 2009, **131**, 15903–15908.

4 S. Fischer, C. Hartl, K. Frank, J. O. Rädler, T. Liedl and B. Nickel, *Nano Lett*, 2016, **16**, 4282–4287.

5 M. Raab, I. Jusuk, J. Molle, E. Buhr, B. Bodermann, D. Bergmann, H. Bosse and P. Tinnefeld, *Sci Rep*, 2018, **8:1780**, 1–11.

6 Alan M. Szalai; Giovanni Ferrari; Lars Richter; Jakob Hartmann; Merve-Zeynep Kesici; Bosong Ji; Kush Coshic; Annika Jaeger; Aleksei Aksimentiev; Ingrid Tessmer; Izabela Kamińska; Andrés M. Vera; Philip Tinnefeld, *biorxiv*.

7 I. Kaminska, J. Bohlen, S. Rocchetti, F. Selbach, G. P. Acuna and P. Tinnefeld, *Nano Lett*, 2019, **19**, 4257–4262.

8 Z. Chen, S. Berciaud, C. Nuckolls, T. F. Heinz and L. E. Brus, *ACS Nano*, 2010, **4**, 2964–2968.

9 T. Cordes, J. Vogelsang and P. Tinnefeld, *J Am Chem Soc*, 2009, **131**, 5018–5019.

10 C. E. Aitken, R. A. Marshall and J. D. Puglisi, *Biophys J*, 2008, **94**, 1826–1835.